1.2

TURBULENCE ANISOTROPY CARRIED BY STREAKS IN THE NEUTRAL ATMOSPHERIC SURFACE LAYER

T. Dubos, P. Drobinski and P. Carlotti
IPSL/LMD, École Polytechnique, France
Ministère de l'Équipement, France

Abstract

We[1] investigate the relationships between coherent structures and turbulence anisotropy in the neutral planetary boundary layer by means of empirical orthogonal function (EOF) analysis of large-eddy simulation (LES) data. The simulated flow contains near-surface transient streaks similar to those revealed by recent observations. The EOF analysis extracts recurrent patterns from the signal based on its second-order spatial correlations. The scale and direction of streaks estimated subjectively from an examination of the LES flow field do correspond to that of the EOFs. The EOF streamlines bear more resemblance with those of optimal perturbations of an Ekman boundary layer than with unstable normal modes.

We find that two characteristics of the turbulence depend in an anisotropic way on the horizontal wave vector of the velocity fluctuations : (i) the vertical extent up to which the turbulent kinetic energy (TKE) is concentrated and (ii) the ratio of the vertical TKE to the horizontal TKE. Although still present in the complete signal, this anisotropy is strongly emphasized by the EOF structures. Furthermore at horizontal wave vectors where recurrent patterns are dominant, the vertical/horizontal TKE ratio is representative of same ratio based on the total flow. This ratio is appreciably far from its isotropic value.

1 INTRODUCTION

Important features of the near-surface turbulence in the neutrally-stratified planetary boundary layer (PBL) are a strong anisotropy and the presence of coherent structures. The relationship between these two features is unclear and the main focus of this work.

In the PBL, the near-surface flow is characterized by transient streaks, which are alternating bands of relatively higher and lower streamwise velocity and are responsible for a significant fraction of the surface stress. The streaks are spatially-periodic linear features of the PBL that reside in the surface layer (SL) and lower portion of the outer-PBL. They are of much smaller scale (wavelengths $\approx$ 100-300 m) than the well-known PBL rolls [Etling and Brown, 1993, Drobinski et al., 1998, Young et al., 2002] and are transient rather than persistent. Streaks appear to go through a continuous cycle of generation, growth, decay and regeneration and typical lifetimes of individual streaks are on the order of tens of minutes [Lin et al., 1996, Foster, 1997, Drobinski and Foster, 2003]. Because they align approximately along the mean shear corresponding to their vertical extent, streaks tend to form at larger angles to the mean wind above the PBL than rolls.

Concomitant with the presence of streaks in the neutral SL, turbulence displays highly anisotropic characteristics: (i) the variances of the wind velocity fluctuations differ for the three components, i.e. $\overline{u^2}/u_\star^2 \simeq 5-6$, $\overline{v^2}/u_\star^2 \simeq 3$ and $\overline{w^2}/u_\star^2 \simeq 1-2$ (where u, v and w are the streamwise, transverse and vertical wind velocity fluctuation and $u_\star$ the friction velocity) or similarly $\overline{v^2}/\overline{u^2}$ and $\overline{w^2}/\overline{v^2}$ are about 0.5 as shown numerically [Moeng and Sullivan, 1994, Drobinski et al., 2006, Grant, 1986, Grant, 1992, Drobinski et al., 2004] and experimentally [Panofsky, 1974], [Nicholls and Readings, 1979]; (ii) close to the ground, the wind velocity spectra show a deviation from the $-5/3$ spectral slope expected for isotropic turbulence with the existence of a -1 power law at intermediate spectral subrange (e.g. [Katul and Chu, 1998] for a review and more recently, [Hunt and Morrison, 2000, Hunt and Carlotti, 2001, Drobinski et al., 2004, Drobinski et al., 2006]).

At the other end on the scale of complexity, the dynamical origin of the rolls and streaks has been investigated in idealized models of the PBL, especially the Ekman flow. Lilly established that the Ekman flow is subject to an inflexion point instability [Lilly, 1966]. The PBL rolls are usually interpreted as the outcome of this instability. More recently, Foster pointed out that optimal perturbations of the Ekman flow present large transient amplifications and that their

[1] *Corresponding author address* : Thomas Dubos, LMD École Polytechnique, 91128 Palaiseau, France ; *E-mail* : dubos@lmd.polytechnique.fr

scale and orientation are in broad agreement with those of near-surface streaks [Foster, 1997]. These linear analyzes lack however all of the nonlinear mechanisms that support turbulence. Especially, the decay of streaks appears to be a nonlinear process [Drobinski and Foster, 2003].

In this paper we investigate the relationship between streaks and turbulence anisotropy in the near-surface flow of a well-resolved large eddy simulation (LES). One major problem is to objectively identify these streaks. Indeed, while organized structures are frequently observed in numerical or field data, they have no unique objective definition and several identification techniques coexist. In vortex identification methods, vortex cores are visualized as isosurfaces of eigenvalues of the velocity gradient, the pressure Hessian and related tensors [Jeong and Hussain, 1995]. Conditional sampling is more quantitative in that it provides the flow and fluxes conditionally averaged with respect to the occurrence of some event, typically ejection or sweep events. Yet it is sometimes criticized on the grounds that the results depend on subjectively chosen sampling criteria. Many studies of PBL coherent structures have used conditional sampling and vortex visualization techniques [Lin et al., 1996, Foster et al., 2006]. References to earlier studies can be found in [Wilson, 1995].

Proper orthogonal decomposition (POD) is an objective extraction technique which has been widely employed on engineering flows [Berkooz et al., 1993]. The outputs are the eigenfunctions of the correlation functions and are unique once a quadratic norm has been chosen. There is often an energetically natural choice of that norm. Furthermore the quadratic quantities can be decomposed into contributions of the individual structures. Hence it is a both quantitative and objective method. Yet its possibilities are much less explored in the geophysical context, except in climatic variability studies where it is known as empirical orthogonal function (EOF) analysis. Apparently only Wilson has applied this method to the PBL [Wilson, 1995, Wilson and Wyngaard, 1995]. He analyzes an LES simulation of a weakly convective PBL in a mesoscale box relevant for rolls spanning most of the PBL. In order to focus on the SL streaks, we analyze a more finely resolved LES in a smaller box [Carlotti, 2002].

Our analysis complements that of Foster et al. based on conditional sampling of the same dataset [Foster et al., 2006]. One major advantage of the EOF analysis is that, due to horizontal homogeneity, it extracts the most recurrent vertical pattern for each horizontal wave vector. The corresponding flows have the same structure as the linear normal modes or optimal perturbations and can be compared to them. Furthermore two aspects of anisotropy can be investigated : (i) the vertical/horizontal ratio of the velocity components and of the extracted flow patterns, and (ii) the dependence of turbulent quantities on the orientation of the horizontal wave vector relatively to the geostrophic wind.

After the introduction in section 1, section 2 presents the data analysis technique. Section 3 describes the individual structures and section 4 investigates their relationship with the anisotropy. Section 5 discusses the results of the EOF analysis and section 6 concludes the study.

2 DATA ANALYSIS

2.1 The dataset

The simulation runs the non-hydrostatic LES model Méso-NH [Lafore et al., 1998] and models a neutrally-stratified atmospheric boundary layer in a box with size (L, l, H) = 3 km × 1 km × 750 m along the x, y, z axes respectively. The mesh cell is a cube of side 6.25 m ($N_x \times N_y \times N_z = 480 \times 160 \times 120$). The subgrid scale (SGS) model is based on a turbulence kinetic energy equation [Cuxart et al., 2000]. However, the simulated flow proved not to be very dependent on the SGS model (Drobinski et al. 2006). The computational box is assumed to be at mid-latitude and a large scale pressure gradient that would balance a geostrophic wind of 10 m s^{-1} above the PBL is imposed. The top of the domain is a rigid lid. The lateral boundary conditions are periodic. At the first grid point above the surface (z = 3.125 m), the wind speed equals $\frac{u_\star}{\kappa}\, log\frac{z}{z_0}$ where $u_\star$ is the friction velocity, $\kappa = 0.4$ is the von Karman constant and z_0 = 10 cm is the roughness length.

The simulation was started from a laminar velocity field in which a very weak random temperature fluctuation ($\Delta T/T \simeq 3 \times 10^{-4}$) was imposed at the bottom of the domain in order to generate turbulence. The temperature fluctuations were quickly damped resulting in a neutrally stratified turbulent flow. Once the flow reached a statistical equilibrium, 14 snapshots of the three dimensional velocity, pressure and the turbulent kinetic energy were extracted and stored, with 500 seconds between each snapshot and each previous snapshot is the initial condition for the next one.

We decompose the velocity field into a mean flow $(U(z), V(z), 0)$ forced by large-scale

pressure gradient and turbulent fluctuations $(u(x,y,z,t),\, v(x,y,z,t),\, w(x,y,z,t))$. In the time-averaged wind hodograph (not shown) the wind is oriented about $12°$ left to the x direction in high layers and about $20°$ left to the long direction close to the ground, following an Ekman spiral continued by a log-layer near the surface. The mean speed profile is approximately logarithmic up to about 270 m. However, there is no appreciable turning in the profile only up to about 40 m, which we take to be the top of the surface layer.

In the first 100 m, the wind fluctuations form streaky structures roughly aligned with the ground wind. These structures appear clearly on horizontal cuts of the velocity field (Fig. 1) and are the dominant features near the surface, associated with an overturning circulation [Foster et al., 2006]. The spacing of the streaks has several apparent scales, from $\approx$ 100 m spacing near the surface and 200 m spacing higher up. The structure of the streaks is broadly consistent with most LES of the neutrally stratified PBL [Deardorff, 1972, Moeng and Sullivan, 1994, Lin et al., 1996, Drobinski and Foster, 2003]. These instantaneous flow realizations clearly show a coherent organization of the turbulence which is not purely wavelike but is an aggregation of smaller-scale structures.

In this neutral flow, $\overline{u^2}/u_\star^2$, $\overline{v^2}/u_\star^2$ and $\overline{w^2}/u_\star^2$ increase between the ground and about $0.02z_i$ (i.e. 15 m) where they reach a maximum, then decrease with height ($\overline{w^2}/u_\star^2$ decrease is much smoother than for the horizontal wind components). The variances $\overline{u^2}/u_\star^2$, $\overline{v^2}/u_\star^2$ and $\overline{w^2}/u_\star^2$ are about 5-6, 3 and 1-2 up to about $0.13z_i$ (i.e. 100 m) [Panofsky, 1974]. The ratios of $\overline{v^2}/\overline{u^2}$ and $\overline{w^2}/\overline{v^2}$ are about 0.5 which is in good agreement with LES studies [Moeng and Sullivan, 1994] and observations [Nicholls and Readings, 1979, Grant, 1986, Grant, 1992, Drobinski et al., 2004]. These ratios tend to 1 near the PBL top. The results of this LES were compared to theoretical developments for two-point statistics [Carlotti, 2002] and integral length-scales [Carlotti and Drobinski, 2004] near the ground and were validated against sonic anemometer and Doppler lidar measurements in the near-neutral surface layer [Drobinski et al., 2006].

We now expose how the EOF analysis permits to recover recurrent patterns from this complex signal.

2.2 Principle of EOF analysis

The principle of EOF analysis, or POD, is the following (see for example [Holmes et al., 1996], chapter 3). Consider a signal represented as an $N-$dimensional real (resp. complex) vector f. Here f will be the deviation of the velocity field from its time average and $N = 3 \times N_x \times N_y \times N_z$. The scalar (resp. Hermitian) product between two vectors is written (f_1, f_2). A natural choice is that (f, f) be the volume-averaged turbulent kinetic energy. A number of snapshots $f_1, \ldots, f_p$ are available, considered as independent realizations of a random vector f, so that it is possible to define an ensemble average $\langle\cdot\rangle$.

The target of EOF analysis is to find vectors $(\phi_1, \ldots, \phi_N)$, called empirical orthogonal functions(EOF), forming an orthonormal basis that optimally represents the signal. By optimally, it is meant that the projection coefficients

$$a_i = (\phi_i^*, f) \text{ such that } f = \sum_i a_i \phi_i \tag{1}$$

have the largest possible variance $\langle |a_i|^2 \rangle$. The self-correlation matrix σ of the signal is the symmetric (resp. Hermitian) positive definite matrix such that for any ϕ:

$$(\phi, \sigma \cdot \phi) = \langle |(\phi, f)|^2 \rangle \tag{2}$$

Hence we want the unit vector ϕ_1 to maximize $(\phi_1, \sigma \cdot \phi_1)$. It is well known that ϕ_1 is then σ's eigenvector with the largest eigenvalue. This eigenvalue is in turn equal to $\langle |a_i|^2 \rangle$, giving the statistical weight of ϕ_1. The second EOF ϕ_2 maximizes $(\phi_2, \sigma \cdot \phi_2)$ in the subspace orthogonal to ϕ_1. Hence it is the eigenvector with the second largest eigenvalue, and so on. In practice the desired number of EOFs can be obtained simultaneously. Finally, the projection coefficients a_i satisfy statistical orthogonality

$$\langle a_i^* a_j \rangle = 0 \quad \text{when} \quad i \neq j,$$

a weak form of mutual statistical independence.

Our set of realizations consists of 14 snapshots of the whole velocity field taken at different instants. Thus this procedure extracts the recurrent spatial flow patterns and drops any temporal or dynamical information from the signal.

2.3 Fourier decomposition

Due to periodic boundary conditions in the x and y directions, it is convenient to write the velocity field in Fourier

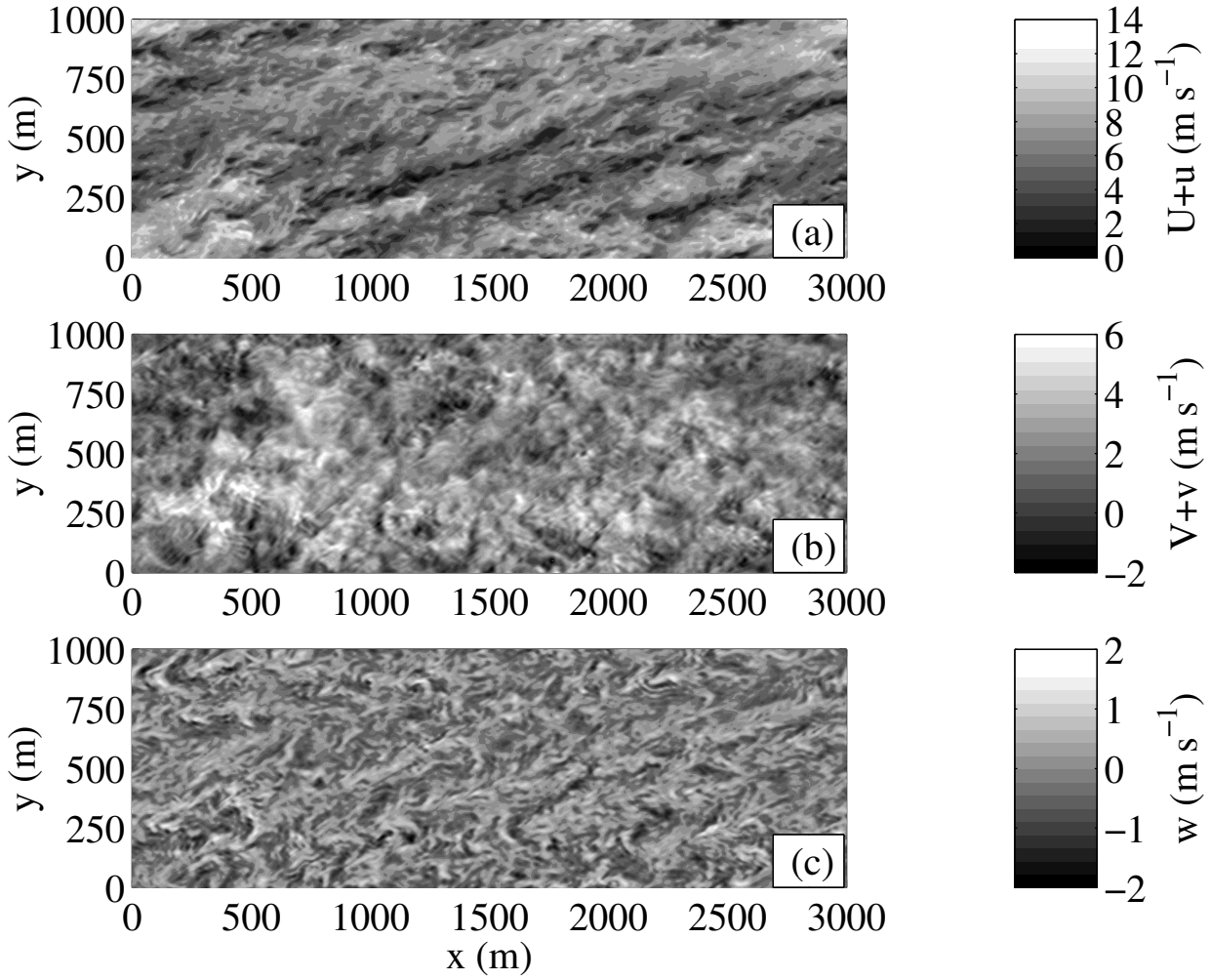

Figure 1: Snapshot of the three velocity components $U+u, V+v, w$ in $m \cdot s^{-1}$ at altitude z = 60 m.

representation :

$$u(x,y,z,t) = Re\sum_{m,n}\hat{u}_{mn}(z,t)\exp 2i\pi\left(\frac{mx}{L}+\frac{ny}{l}\right)$$

where the horizontal wave-vector $(k_x, k_y) = 2\pi(m/L, n/l)$ is quantized according to the box dimensions L and l. Assuming statistical invariance on horizontal translations, the cross-correlation between Fourier coefficients $\hat{u}_{mn}(z,t)$ with different wave vectors is zero. The eigenvalue problem is then local to each Fourier mode.

As the scalar product underlying the EOF analysis, we choose the box-averaged turbulent kinetic energy $\int(\hat{u}\hat{u}^* + \hat{v}\hat{v}^* + \hat{w}\hat{w}^*)\,\mathrm{d}z/H$. Hence for each m,n we compute the self-correlation matrix $\sigma^{mn}(k_x,k_y)$. This is a $3N_z \times 3N_z$ matrix made of $N_z \times N_z$ blocks. Each 3×3 block contains the correlations between two altitudes z and z' among the $N_z = 120$ resolved by the model :

$$\left\langle \begin{array}{ccc} \hat{u}^*_{mn}(z)\hat{u}_{mn}(z') & \hat{v}^*_{mn}(z)\hat{u}_{mn}(z') & \hat{w}^*_{mn}(z)\hat{u}_{mn}(z') \\ \hat{u}^*_{mn}(z)\hat{v}_{mn}(z') & \hat{v}^*_{mn}(z)\hat{v}_{mn}(z') & \hat{w}^*_{mn}(z)\hat{v}_{mn}(z') \\ \hat{u}^*_{mn}(z)\hat{w}_{mn}(z') & \hat{v}^*_{mn}(z)\hat{w}_{mn}(z') & \hat{w}^*_{mn}(z)\hat{w}_{mn}(z') \end{array} \right\rangle .$$

The eigenvalues E_i^{mn} and eigenvectors $(\hat{u}_i^{mn}(z), \hat{v}_i^{mn}(z), \hat{w}_i^{mn}(z))$ of the $3N_z \times 3N_z$ Hermitian matrix σ^{mn} finally provide the desired EOFs and their energetic weight. The corresponding flow patterns have a vertical structure described by $(\hat{u}_i^{mn}(z), \hat{v}_i^{mn}(z), \hat{w}_i^{mn}(z))$ and a sinusoidal horizontal dependence. We sort the energies E_i^{mn} in descending order $E_1^{mn} > E_2^{mn} > \ldots$ Notice that by construction, $E^{mn} = \sum_i E_i^{mn}$ is exactly the spectral density of turbulent kinetic energy for the horizontal wave vector (k_x,k_y).

2.4 Decomposition property

At each wave vector, the ratio E_1^{mn}/E^{mn} called energy fraction explained by the first $(i=1)$ EOF is an indicator of the statistical significance of the first EOF. Suppose for instance that for a given wave vector $E_1^{mn}/E^{mn} = 1$. Then all projection coefficients a_i with $i > 1$ must be zero in the decomposition given by Eq. (1). Thus the flow (within this Fourier mode) has the same vertical structure at all instants, but appears with a random amplitude given by $|a_1|$ and at a random position given by the phase of a_1. Conversely, if the energy is equipartitioned among all EOFs, the signal is white-in-space noise. So only wave vectors with a significant explained energy fraction can be said to be "strongly structured" and present recurrent patterns.

Due to the statistical orthogonality of the projection coefficients a_i any quantity that depends quadratically on the signal can on average be split into individual contributions from the EOFs. Quadratic quantities of particular interest here are the turbulent kinetic energy and the shear production of turbulent kinetic energy.

The horizontally-averaged turbulent kinetic energy $e(z,t)$ and shear production $S(z,t)$ can first be written as the sum of contributions from each Fourier mode:

$$\begin{aligned} e(z,t) &= \int\int \left(u^2+v^2+w^2\right)\frac{\mathrm{d}x\mathrm{d}y}{2Ll} \\ &= \sum_{mn} e^{mn}(z,t) \\ e^{mn}(z,t) &= \left(\hat{u}_{mn}\hat{u}^*_{mn} + \hat{v}_{mn}\hat{v}^*_{mn} + \hat{w}_{mn}\hat{w}^*_{mn}\right)/2 \end{aligned}$$

$$\begin{aligned} S(z,t) &= \int\int w\left(u\frac{\mathrm{d}U}{\mathrm{d}z}+v\frac{\mathrm{d}V}{\mathrm{d}z}\right)\frac{\mathrm{d}x\mathrm{d}y}{Ll} \\ &= \sum_{mn} S^{mn}(z,t) \\ S^{mn}(z,t) &= Re\left(\left(\hat{u}_{mn}\frac{\mathrm{d}U}{\mathrm{d}z}+\hat{v}_{mn}\frac{\mathrm{d}V}{\mathrm{d}z}\right)\hat{w}^*_{mn}\right) \end{aligned}$$

The quadratic quantities e^{mn} and S^{mn} may then be decomposed on average into contributions from the individual EOFs:

$$\begin{aligned} \langle e^{mn}(z,t)\rangle &= \sum_i E_i^{mn} e_i^{mn}(z) \\ e_i^{mn}(z) &= \frac{|\hat{u}_i^{mn}(z)|^2 + |\hat{v}_i^{mn}(z)|^2 + |\hat{w}_i^{mn}(z)|^2}{2} \end{aligned}$$

$$\begin{aligned} \langle S^{mn}(z,t)\rangle &= \sum_i E_i^{mn} S_i^{mn}(z) \\ S_i^{mn}(z) &= Re\left(\left(\hat{u}_i^{mn}\frac{\mathrm{d}U}{\mathrm{d}z}+\hat{v}_i^{mn}\frac{\mathrm{d}V}{\mathrm{d}z}\right)\hat{w}_i^{mn*}\right) \end{aligned}$$

3 SIGNIFICANCE AND FLOW STRUCTURE OF THE EXTRACTED PATTERNS

3.1 Significant EOFs

We display in Fig. 2 the energy fraction E_1^{mn}/E^{mn} explained by the first $(i=1)$ EOF at each wave vector. We consider that when the energy fraction explained by the first EOF exceeds a threshold of $\geq 50\%$, then the wave

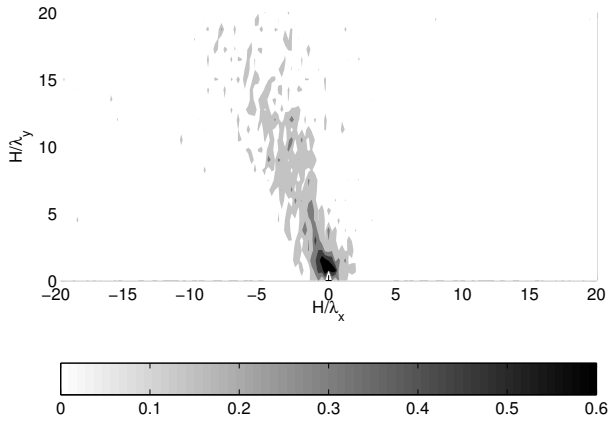

Figure 2: Energy fraction E_1^{mn}/E^{mn}explained by the first EOF of each Fourier mode as a function of the wave vector $\mathbf{k} = 2\pi(m/L, n/l)$.

vector is significant. The choice of the threshold is somewhat arbitrary but does not affect the qualitative shape of the spectral domain where wave vectors are significant. Wave vectors with a significant explained energy fraction lie all in a narrow range of the Fourier space close the line $m+n=0$. These Fourier modes have their phase lines nearly parallel to the surface wind, in agreement with qualitative observation of streaks.

We shall consider and compare the contributions due to four sets of EOFs:

- the set $A = (\hat{u}_i^{mn}(z), \hat{v}_i^{mn}(z), \hat{w}_i^{mn}(z))_{imn}$ for all i,m,n. Set A consists of all EOFs in all Fourier modes and its contribution is by definition the average over the full flow field.
- the set $B = (\hat{u}_1^{mn}(z), \hat{v}_1^{mn}(z), \hat{w}_1^{mn}(z))_{mn}$ for all m,n. Set B consists of the dominant EOF in each Fourier mode.
- the set $C = (\hat{u}_i^{-m,m}(z), \hat{v}_i^{-m,m}(z), \hat{w}_i^{-m,m}(z))_{i,m}$ for all i,m. Set C consists of all EOFs in the line of Fourier modes such that $m+n=0$ and identified as "strongly structured". The contribution of this set to quadratic quantities is equal to the spectral contribution of these particular modes.
- the set $D = (\hat{u}_1^{-m,m}(z), \hat{v}_1^{-m,m}(z), \hat{w}_1^{-m,m}(z))_m$ for all m. Set D consists of the dominant EOF of each "strongly structured" Fourier mode.

Hence the sets B and C are distinct subsets of A , and D is the intersection of sets B and C.

3.2 Energy and turbulent fluxes

In order to quantify the actual weight of the extracted structures, we display the contributions of sets A, B, C, and D to the vertical profiles of turbulent kinetic energy and of shear production of energy (Fig. 3). Let us first compare sets C and D. By definition, the set D is made of the most energetic EOFs of set C. This reflects onto their respective contribution to the TKE and shear production : although it consists of much fewer EOFs, set D contributes to an amount of the same order of magnitude as set C. Let us now compare sets C and A. Set C covers only a small fraction of the spectral space and contributes modestly to the overall profile corresponding to set A. Figure 3 emphasizes the fact that the contribution of set C is an order of magnitude smaller that the total. Finally, it is interesting to compare the contributions due to set B to the complete average, corresponding to set A. Indeed, set B is to set A what set D is to set C : it contains only one EOF (the most energetic) at each wave-vector. However because most wave-vectors are weakly structured (do not present recurrent patterns), by ignoring all but one EOF at each wave-vector one also drops a lot of the velocity fluctuations. As a result, while the contributions of sets C and D are of the same order of magnitude, the contribution of set B is several times smaller than the complete average (set A).

3.3 Typical flow structure

Due to incompressibility, the flow corresponding to a single Fourier mode or to several Fourier modes with parallel wave vectors can be conveniently described in terms of an across-wave-vector horizontal (along-roll, downstream) velocity u' and an along-wave-vector stream function, from which the vertical velocity w and the along-wave-vector horizontal velocity v' are derived. This description and choice of axes is called Squire's transformation in the context of normal-mode stability analysis [Foster, 1997].

The first EOFs are found to be concentrated close to the ground with a vertical extension comparable to their horizontal wavelength. At very low wave-numbers ($-m=n=1,2$), the vertical scale of the EOFs is about $200 \sim 400$ m, quite too large for streaks. Higher-wavenumber EOFs ($-m=n=4,5$) are more likely to correspond to the

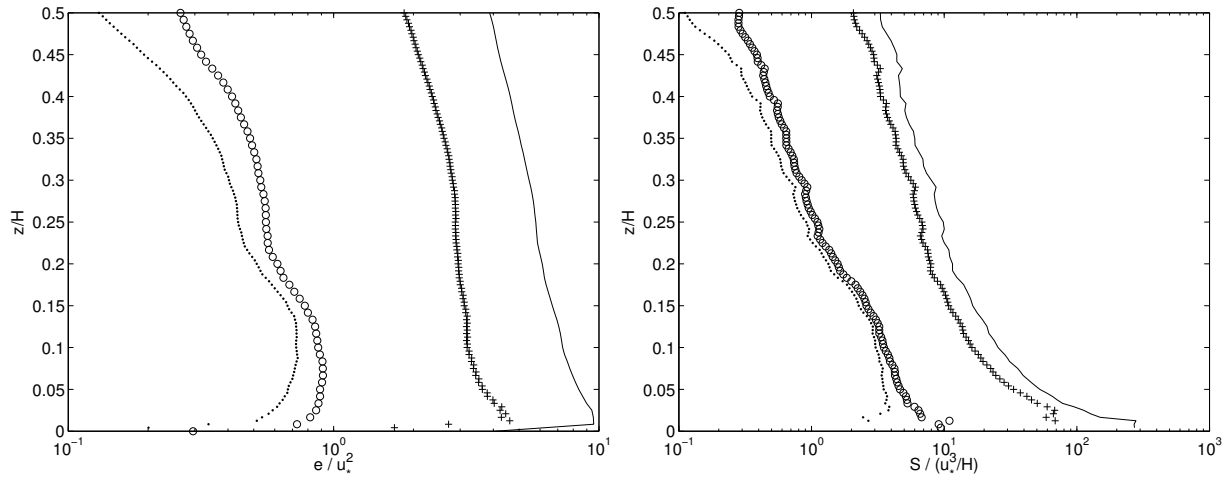

Figure 3: Contribution of sets of EOFs A (solid), B (crosses), C (circles) and D (dots) to the profiles of turbulent kinetic energy $e(z)$ (left) and shear production of energy $S(z)$ (right).

streaks (Fig. 4). Both have the structure of an alternating along-roll jet superimposed onto two counter-rotating rolls typical of linearly unstable normal modes and of optimal perturbations [Foster, 1997]. The stream function is approximately in quadrature with respect to the along-roll velocity. This means that the along-roll and vertical velocities are roughly in phase, producing on average a vertical flux of horizontal momentum and extracting energy from the mean shear. Compared to the downstream velocity, the stream function of the linearly most unstable normal mode extends vertically roughly twice as much ([Foster, 1997], fig. 4). At contrast the downstream velocity and stream function of the optimal perturbations have roughly the same vertical extent. ([Foster, 1997], figs 7-8). The patterns presented in Fig. 4 thus bear more resemblance to the optimal perturbations than to the unstable normal modes.

We finally display for the Fourier modes $-m = n = 2$ and $-m = n = 4$ the vertical profiles of kinetic energy $e_1^{mn}(z)$ (Fig. 5) and of production rate of energy by the shear (Fig. 5). Since EOFs have by construction unit norm, $e_1^{mn}(z)$ is a non-dimensional quantity whose $z-$average is 1. It can be seen that the energy of the first EOF is concentrated closer to the ground than the total energy of the corresponding Fourier mode. Concerning the shear production, most of it is solely due to the first EOF. Only very close to the ground does the flux intensity contributed by the first EOF decrease much faster than the total contribution by the corresponding Fourier mode. The maximum shear production for the first EOF of Fourier mode $(-m = n = 4)$ is attained at an altitude $\simeq 0.08 z_i$ (i.e. about 60 m) which corresponds to the typical altitude up to which streaks can be qualitatively observed in this LES.

The EOF technique is therefore successful at (i) identifying objectively the horizontal characteristics of the recurrent flow patterns (wavelength and orientation) (ii) providing the corresponding vertical structure of the flow. However when further analyzing results based on this analysis, one must bear in mind that the recurrent patterns extracted by the EOF technique represent only a small fraction of the energy (except, by construction, in the "strongly structured" spectral domain).

4 ANISOTROPY

4.1 Vertical extent

The vertical extent of rolls or streaks is often studied by investigating up to which height above ground the spatial features of a horizontal cut ($z = const$) of the velocity field survive. Here because the EOFs precisely represent the correlations between the different altitudes, the different levels are never considered independently. Therefore we characterize the vertical extent of the turbulent structures through their TKE center, the column average of altitude

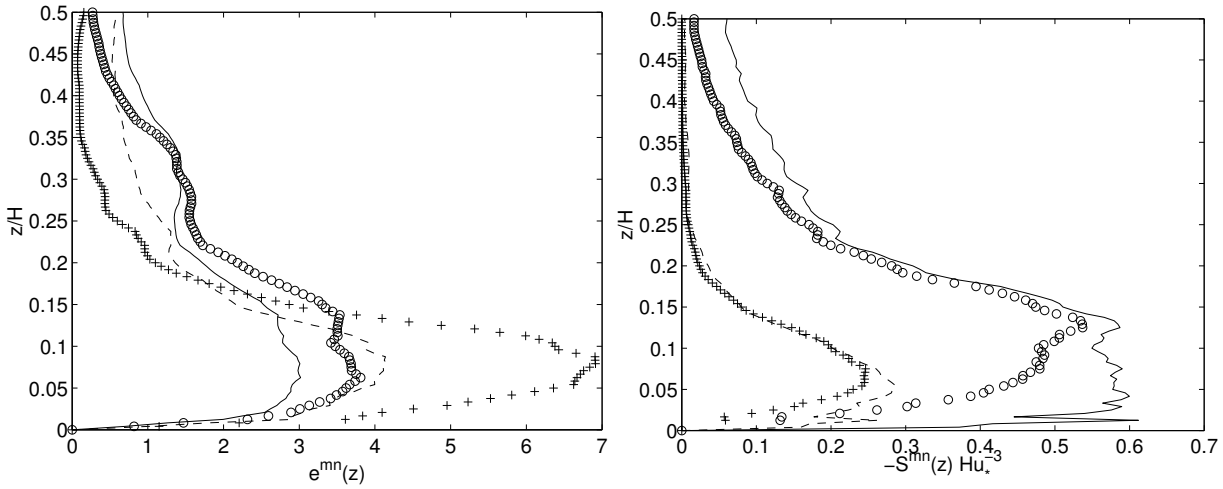

Figure 5: Left : vertical repartition e_1^{mn} of the kinetic energy of the first EOFs for Fourier modes $-m = n = 2$ (circles) and $-m = n = 4$ (crosses) ; vertical repartition e^{mn} of the total kinetic energy contained in the Fourier modes $-m = n = 2$ (solid) and $-m = n = 4$ (dashed).
Right : vertical profile of $-S_1^{mn}$ (contribution of the first EOFs to the shear production) for Fourier modes $-m = n = 2$ (circles) and $m = -n = 4$ (crosses); vertical profile of the total shear production S^{mn} for the Fourier modes $-m = n = 2$ (solid) and $-m = n = 4$ (dashed)

weighted by the turbulent kinetic energy :

$$Z^{mn} = \frac{\int z e^{mn}(z) \mathrm{d}z}{\int e^{mn}(z) \mathrm{d}z}$$

In this definition, one can choose to weigh by the total TKE or only by the horizontal TKE $e_H = \frac{1}{2}(u^2 + v^2)$ or the vertical TKE $e_V = \frac{1}{2}w^2$. In addition, the velocity components can be either those of a given Fourier mode $(\hat{u}^{mn}, \hat{v}^{mn}, \hat{w}^{mn})$ or those of an EOF $(\hat{u}_i^{mn}, \hat{v}_i^{mn}, \hat{w}_i^{mn})$. The height Z^{mn} can then be interpreted as a penetration height up to which a given Fourier mode or EOF contributes significantly to its part of the more commonly used horizontal Fourier spectrum.

We display in Fig. 6 the TKE center as a function of the horizontal wavenumber, obtained from the horizontal energy e_H^{mn} of the corresponding Fourier mode (panel a) or obtained from the horizontal energy e_{H1}^{mn} of the corresponding EOF only (panel b). A global trend is that horizontally short structures (large wave-vectors) have a correspondingly small vertical extent. A striking feature is the strong anisotropy in the values of the TKE center Z. For wave vectors lying on the line $m + n = 0$, the TKE center is much smaller than that of wave vectors of comparable magnitude and different direction. This anisotropy is more pronounced for the TKE center based on EOFs (panel b). The line $m + n = 0$ corresponds to the strongly structured wave vectors. Hence what we observe is that the most recurrent patterns of this flow are more concentrated close to the ground than the more disordered motions of comparable horizontal scale.

Considering finally the TKE center obtained now from the vertical energy e_V^{mn} (not shown), the trend that horizontally short structures have a small vertical extent persists. However the anisotropy in the values of the TKE center Z_{mn} is much less apparent, yet still visible for the TKE center based on EOFs. Now, the vertical velocity is blocked near the ground, which is not the case for the horizontal components (above the thin viscous sublayer). The strength of this blocking effect of this effect does not depend on the direction of the wave vector. Hence it may be the origin of the weaker dependence of the vertical TKE on the direction of the horizontal wave-vector.

4.2 Vertical vs horizontal turbulent kinetic energy

We have discussed so far the anisotropic dependence of the vertical extent of flow patterns on their horizontal wave

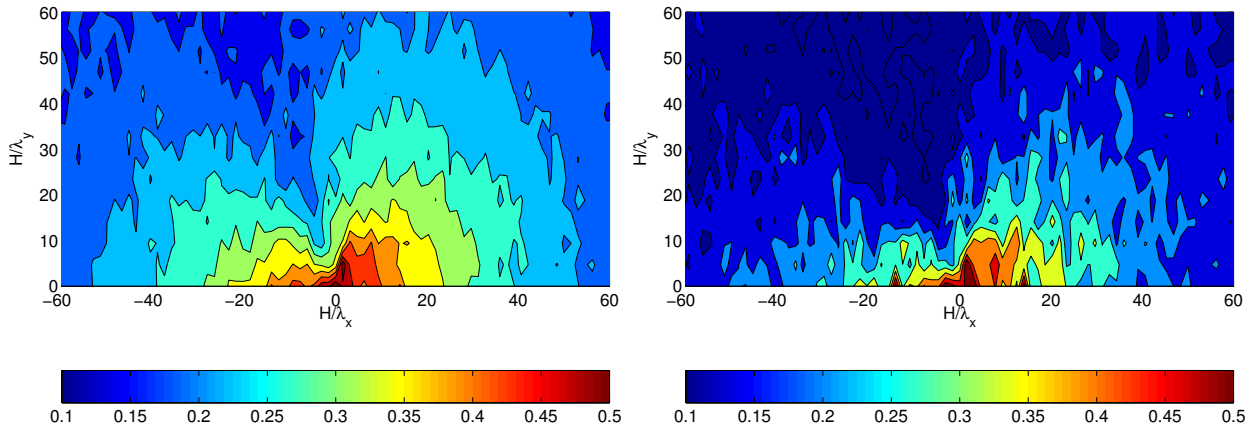

Figure 6: TKE center Z^{mn} as a function of the horizontal wave vector $\mathbf{k} = (2\pi/\lambda_x, 2\pi/\lambda_y)$.Left : weighted by the horizontal TKE of each Fourier mode. Right : weighted by the horizontal TKE of each first EOF.

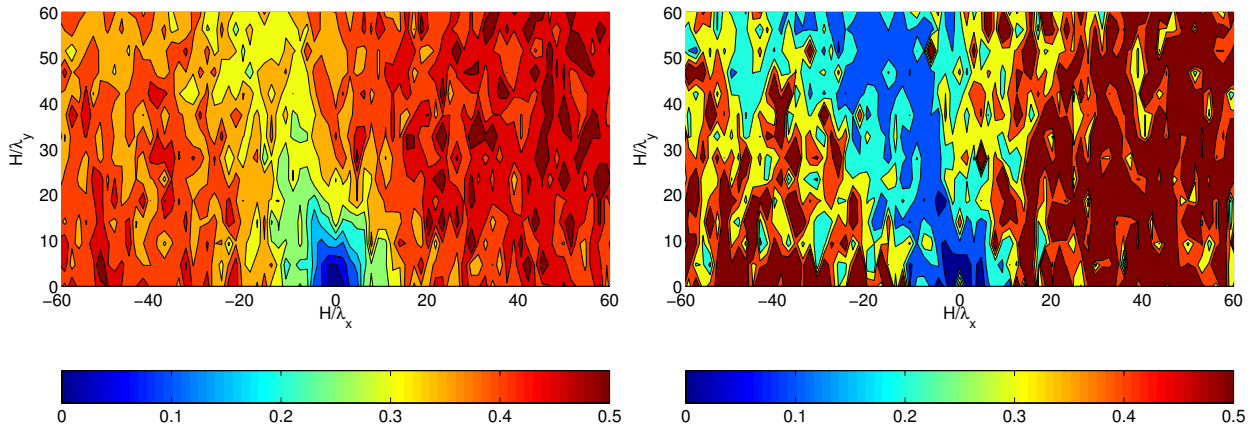

Figure 7: Ratio e_V/e_H of vertical to horizontal TKE. (a) vertically averaged TKEs. (b) only the contribution due to the first EOF.

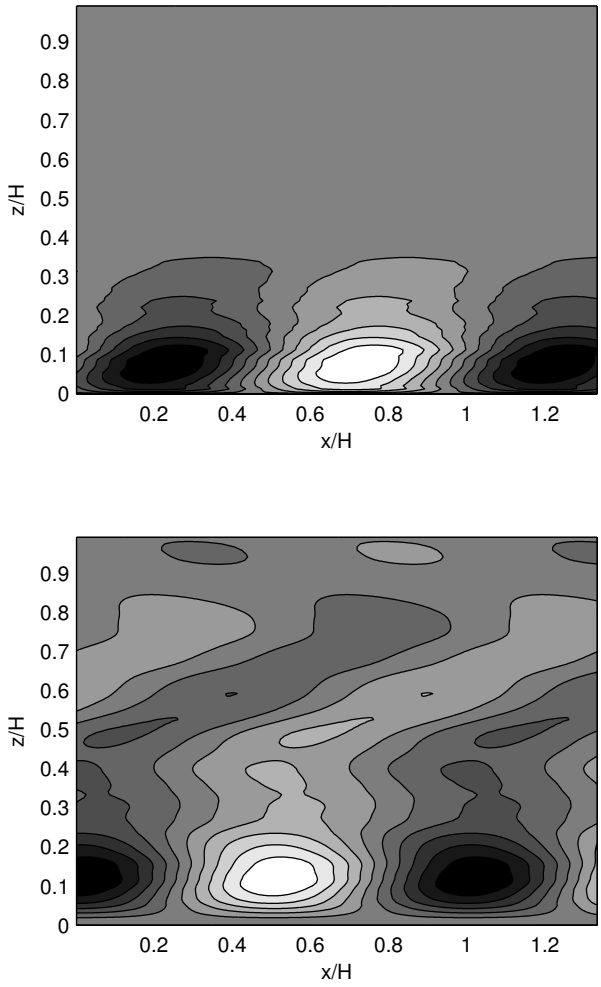

Figure 4: Flow structure of the first EOF at wave-vector $\mathbf{k} = 2\pi(-4/L, 4/l)$. The horizontal axis is parallel to the wave-vector. Top : contours of cross-wave-vector (along-roll) velocity. Bottom : contours of along-wave-vector stream function (regularly spaced).

vector. Anisotropy may enter in a second way for a vector quantity such as velocity since it may point in directions that are not isotropically distributed. An indication of that is given by the ratio e_V/e_H of the vertical TKE over the horizontal TKE. The properties of homogeneous and isotropic turbulence are that (i) the ensemble means associated with the turbulent state are invariant with respect to any translation, rotation or symmetry; (ii) in practice, there is no privileged direction for turbulence. If the velocity fluctuations had isotropically distributed directions, as in locally isotropic turbulence, this ratio would be equal to $1/2$ ($\overline{u^2} = \overline{v^2} = \overline{w^2}$).

We display in Fig. 7a the TKE ratio e_V/e_H as a function of the horizontal wavenumber. Only for very small scales (large wave vectors) does e_V/e_H approach the isotropic value of $1/2$. Everywhere else the TKE ratio is in favor of the horizontal TKE, especially at large horizontal scales (small wave vectors) but also and more remarkably for "strongly structured" wave vectors (lying on the line $m+n=0$). Figure 7b presents the ratio e_{V1}/e_{H1} of the contribution of the first EOF to the vertical and horizontal TKEs. Retaining only the first EOFs worsens the statistical convergence, resulting in a more noisy plot. Nevertheless the features discussed above are clearly visible in an even more pronounced way. In a narrow angular sector containing the "strongly structured" line $m+n=0$, the TKE ratio is in favor of the horizontal TKE while it is much closer to its isotropic value of $1/2$ outside this sector.

One expects isotropy to be violated by very large scale structures since their vertical extent is limited by the PBL depth, resulting in a low geometric aspect ratio. Because of incompressibility, such structures with small vertical extent relatively to their horizontal scale have a correspondingly low vertical velocity. Conversely, horizontally short structures are free to achieve a vertical/horizontal aspect ratio of 1 or more and the corresponding ratio of vertical to horizontal TKE. This is clearly not the case at "strongly structured" wave vectors for which a typical e_V/e_H ratio is about 0.2 even at large wave vectors. This is consistent with the observation that the corresponding flow patterns are closer to the ground that those of equivalent horizontal scale and different direction, resulting in a lower vertical/horizontal aspect ratio. Noticing that for the total signal, $\overline{v^2}/\overline{u^2}$ and $\overline{w^2}/\overline{v^2}$ are about 0.5, we obtain that $e_V/e_H \simeq 0.17$ which is remarkably similar to the ratio found for the "strongly structured" wave vectors. Hence the "strongly structured" wave vectors carry a turbulence anisotropy that is representative of the anisotropy observed in the total sig-

nal.

5 SUMMARY

We have analyzed a dataset produced by a large-eddy simulation (LES) of a neutral atmospheric surface layer (SL). In the LES, the small-scale streaks can be observed up to about $0.13z_i$ (i.e. 100 m above the ground). We have performed an empirical orthogonal function (EOF) analysis, which is in substance a more convenient way to represent the statistical information contained in the correlation matrix, particularly here the correlations between the velocity fluctuations at different altitudes. This is at contrast with, for instance, a level-by-level spectral analysis, which would discard these correlations. Furthermore the extracted EOFs have a flow structure similar to that of linearly unstable normal modes and optimal perturbations. EOF analysis thus provides a way to compare features emerging from complex, fully nonlinear dynamics and idealized, linearized dynamics.

A number of interesting observations were made possible by the EOF analysis:

- not all horizontal wave-vectors, rather few in fact, present recurrent patterns in their vertical profile. We identified the narrow band in the Fourier space near $m+n=0$ where such recurrent patterns are strong enough that the first EOF carries significantly larger energy than the next ones. The orientation of this band is in agreement with a qualitative feeling of the streak lines. Thus these patterns are indeed produced by structures with a spatial coherence on the vertical.

- the corresponding structure of the turbulence is strongly altered. For a horizontal wave vector belonging to this narrow band, the turbulence extends on a vertical range much smaller than for wave vectors with comparable magnitude and unspecified direction. This observation is particularly true for the fluctuations of horizontal velocity (as measured by the horizontal turbulent kinetic energy) and less for vertical velocity.

- the velocity fluctuations are also distributed in a less isotropic way, as made apparent by the depleted ratio of vertical and horizontal turbulent kinetic energies.

These last two points are strongly emphasized when the signal is projected onto the most energetic EOF of each Fourier mode, but still convincingly present in the complete signal. This is important since the dominant EOFs finally account for a relatively small fraction of the total kinetic energy. The significance of properties of the EOF-filtered signal could therefore be questionable. Here we use the EOF analysis to point us at the regions of Fourier space where coherent structures are important and might have a signature on the turbulence, but rely on both the EOF-filtered signal and the complete signal to characterize this signature.

Acknowledgements

The authors would like to thank J.-L. Redelsperger, H.~Adanfari and R.C. Foster for fruitful discussions; M.C. Lanceau for help in collecting the referenced papers. The LES was done thanks to a funding of the French Ministry for Transportation and Météo France. This research has also been funded by the Centre National de Recherche Scientifique (CNRS) and the Institut des Sciences de l'Univers (INSU) through the Programme ATmosphère Océan à Multi-échelle (PATOM).

References

[Berkooz et al., 1993] Berkooz, G., Holmes, P., and Lumley, J. (1993). The proper orthogonal decomposition in the analysis of turbulent flows. *Ann. Rev. Fluid Mech.*, 25:539–575.

[Carlotti, 2002] Carlotti, P. (2002). Two-point properties in atmospheric turbulence very close to the ground : comparison of a high resolution LES with theoretical models. *Bound.-Layer Meteor.*, 104:381–410.

[Carlotti and Drobinski, 2004] Carlotti, P. and Drobinski, P. (2004). Length-scales in wall-bounded high reynold s number turbulence. *J. Fluid Mech.*, 516:239–264.

[Cuxart et al., 2000] Cuxart, J., Bougeault, P., and Redelsperger, J.-L. (2000). A multiscale turbulence scheme apt for LES and mesoscale modelling. *Quart. J. Roy. Meteorol. Soc.*

[Deardorff, 1972] Deardorff, J. (1972). Numerical Investigation of Neutral and Unstable Planetary Boundary Layer. *J. Atoms. Sci.*, 29:91–115.

[Drobinski et al., 1998] Drobinski, P., Brown, R., Flamant, P., and Pelon, J. (1998). Evidence of organized large eddies by ground-based doppler lidar, sonic anemometer and sodar. *Bound.-Layer Meteor.*, 88:343–361.

[Drobinski et al., 2004] Drobinski, P., Carlotti, P., Newson, R., Banta, R., Foster, R., and Redelsperger, J.-L. (2004). The structure of the near-neutral atmospheric surface layer. *J. Atmos. Sci.*, 61(699-714).

[Drobinski et al., 2006] Drobinski, P., Carlotti, P., Redelsperger, J.-L., Banta, R., Masson, V., and Newsom, R. (2006). Numerical and experimental investigation of the neutral atmospheric surface layer. *J. Atmos. Sci. (in revision)*.

[Drobinski and Foster, 2003] Drobinski, P. and Foster, R. (2003). On the origin of near-surface steaks in the neutrally-stratified planetary boundary layer. *Boundary-Layer Meteorol.*, 108:247–256.

[Etling and Brown, 1993] Etling, D. and Brown, R. (1993). Roll vortices in the planetary boundary layer: a review. *Bound.-Layer Meteor.*, 21:215–248.

[Foster, 1997] Foster, R. (1997). Structure and energetics of optimal Ekman layer perturbations. *J. Fluid. Mech.*, 333:97–123.

[Foster et al., 2006] Foster, R., Vianney, F., Drobinski, P., and Carlotti, P. (2006). Near-surface coherent structures and the momentum flux in a large eddy simulation of neutrally-stratified boundary layer. *Bound.-Layer Meteor. (submitted)*.

[Grant, 1986] Grant, A. (1986). Observations of boundary layer structure made during the 1981 kontur experiment. *Quart. J. Roy. Meteor. Soc.*, 112(825-841).

[Grant, 1992] Grant, A. (1992). The structure of turbulence in the near-neutral atmospheric boundary layer. *J. Atmos. Sci.*, 49:226–239.

[Holmes et al., 1996] Holmes, P., Lumley, J., and Berkooz, G. (1996). *Turbulence, Coherent Structures, Dynamical Systems and Symmetry*. Cambridge University Press.

[Hunt and Carlotti, 2001] Hunt, J. and Carlotti, P. (2001). Statistical structure at the wall of the high reynolds number turbulent boundary layer. *Flow, Turbulence and Combustion*, 66:453–475.

[Hunt and Morrison, 2000] Hunt, J. and Morrison, J. (2000). Eddy structure in turbulent boundary layers. *Eur. J. Mech. B - Fluids*, 19:673–694.

[Jeong and Hussain, 1995] Jeong, J. and Hussain, F. (1995). On the identification of a vortex. *J. Fluid Mech.*, 285(69).

[Katul and Chu, 1998] Katul, G. and Chu, C. (1998). A theoretical and experimental investigation of the energy-containing scales in the dynamic sublayer of boundary-layer flows. *Bound.-Layer Meteorol.*, 86:279–312.

[Lafore et al., 1998] Lafore, J., Stein, J., Asencio, N., Bougeault, P., Ducrocq, V., Duron, J., Fischer, C., Héreil, P., Mascart, P., Masson, V., Pinty, J.-P., Redelsperger, J.-L., Richard, E., and Vilà-Guerau de Arellano, J. (1998). The Méso-NH atmospheric simulation system. Part I: adiabatic formulation and control simulation. *Ann. Geophys.*, 16:90–109.

[Lilly, 1966] Lilly, D. (1966). On the instability of Ekman boundary flow. *J. Atmos. Sci.*, 23(481-494).

[Lin et al., 1996] Lin, C.-L., McWilliams, J., Moeng, C.-H., and Sullivan, P. (1996). Coherent Structures in a Neutrally-Stratified Planetary Boundary Layer. *Phys. Fluids*, 8:2626–2639.

[Moeng and Sullivan, 1994] Moeng, C. and Sullivan, P. (1994). A Comparison of Shear- and Buoyancy-Driven Planetary Boundary Layer Flows. *J. Atmos. Sci.*, 51:999–1022.

[Nicholls and Readings, 1979] Nicholls, S. and Readings, C. (1979). Aircraft observations of the structure of the lower boundary layer over the sea. *Quart. J. Roy. Meteor. Soc.*, 107:785–802.

[Panofsky, 1974] Panofsky, H. (1974). The atmospheric boundary layer below 150 meters. *Ann. Rev. Fluid Mech.*, 6:147–177.

[Wilson, 1995] Wilson, D. (1995). Empirical Orthogonal Function analysis of the weakly convective atmospheric boundary layer. Part I : Eddy Structures. *J. Atmos. Sci.*, 53(6):801–823.

[Wilson and Wyngaard, 1995] Wilson, D. and Wyngaard, J. (1995). Empirical Orthogonal Function analysis of the weakly convective atmospheric boundary layer. Part II : Eddy Energetics. *J. Atmos. Sci.*, 53(6):824–841.

[Young et al., 2002] Young, G., Kristovich, D., Hjelmfelt, M., and Foster, R. (2002). Rolls, streets, waves and more: a review of quasi-two dimensional structures in the atmospheric boundary layer. *Bull. Amer. Meteor. Soc.*, 83:997–1001.